Journal of University of Babylon for Engineering Sciences, Vol. (26), No. (9): 2018.

Synthesis and Characterization of Zno Nanoparticles Using Hydrothermal and Sol-Gel Techniques for Dye-Sensitized Solar Cells

H. Musleh[1, 2,*] N. AlDahoudi[2] H. Zayed[1] S. Shaat[3] H. M. Tamous[4] N. Shurrab[4] A. Issa[5] J. Asad[2]

[1]Physics Department, Women`s College for Art, Science, and Education, Ain Shams University, Cairo, Egypt

[2]Science, Physics Department, Al Azhar University-Gaza, Gaza, Palestine, P.O. Box 1277

[3] Physics Department, Islamic University of Gaza, Science, Gaza, Palestine, P.O. Box 108.

[4]Chemistry Department, Alzhar University-Gaza, Science, Gaza, Palestine, P.O. Box 1277

[5]Engineering Department, Azhar University-Gaza, Science, Gaza, Palestine, P.O. Box 1277

h.mphysics@hotmail.com

Submission date:- 11/9/2018	Acceptance date:- 11/10/2018	Publication date:- 4/11/2018

Abstract

ZnO nanoparticles (ZnO NPs) were synthesized using hydrothermal and sol-gel techniques using zinc acetate dihydrate (Zn $(CH_3COO)_2.2H2O$) as a row material and methanol as a solvent. The structural properties of ZnO NPs were studied using EDX, XRD, TEM, and the optical properties were characterized using UV-VIS and PL spectroscopies. The synthesized ZnO NPs showed high purity and revealed a wurtzite (hexagonal) crystal structure with particle size (D) ranged from 25 nm to 28 nm. The UV-VIS absorption spectra of ZnO NPs samples and sensitizing dyes were performed. The obtained ZnO NPs exhibited the direct optical bandgap 3.15 eV. Dye-sensitized solar cells (DSSCs) were fabricated using synthesized ZnO NPs as a semiconducting layer, which was dyed with different low cost dyes such as Eosin B (EB), Eosin Y (EY) and Rhodamine B (RB) that was used to sensitize the photoanode (ZnO NPs). The experimental results showed a significant efficiency for the fabricated DSSCs of synthesized ZnO NPs via sol gel technique comparing to hydrothermal technique. The EY dye exhibited the best performance among others, where a conversion efficiency showed a noteworthy improvement from 0.12 to 1.08 %.

Keywords: ZnO NPs, Hydrothermal, Sol gel, PL and DSSCs.

1- Introduction

Zinc Oxide nanoparticles (ZnO NPs) is a versatile material with multifunctional properties such as high chemical stability, high photostability, low dielectric constant, and good UV absorption material [1]. In recently years, the interests in synthesis and characterization of ZnO NPs for specific properties has increased extremely [2]. ZnO is an excellent semiconductor material, due to its large bandgap (3.37 eV) for applications considered for other wide bandgap [3, 4]. It has been found that ZnO can be used in other potential applications such as DSSCs (dye sensitized solar cell)[5], medical purposes[6] and photocatalysis[7], which making them exciting commodities for industries. In addition, the excitons in ZnO are thermally stable at room temperature due to the extremely large exciton binding energy (about 60 meV) [8]. Currently, various approaches have been used to synthesis ZnO NPs with different characteristics such as radio frequency sputtering (RFS)[9], chemical vapor deposition (CVD) [10, 11], pulse laser deposition (PLD)[12], spray pyrolysis[13], sol-gel method [14], solution combustion method [15], hydrothermal method [16, 17], and reflux method [18]. In this work, a comparative study between two different techniques hydrothermal (HT) and sol–gel (SG) were investigated to synthesize ZnO NPs. The structure and the optical properties of the prepared samples were reported. Additionally, DSSCs were fabricated using synthesized samples (HT) and (SG) as a photoanode. Three chemical dyes contains Xanthene group: Eosin Y (EY), Eosin B (EB) and Rhodamine B (RB) as metal-free organic (MFODs) low price sensitizing dyes to make certain the benefits of the xanthene dyes as suitable candidates to replace Ru-based dyes in ZnO based cells. The J-V characteristic curves for the fabricated solar cells were tested and analyzed. The photovoltaic parameters related to the solar cell performance were determined.

2 Experimental Procedure

2.1 Synthesis of ZnO Nanoparticles

- **Hydrothermal Method**

Hydrothermal (HT) method was used to synthesize the ZnO NPs[19]. 4 g of zinc acetate dihydrate, $Zn(CH_3COO)_2.2H_2O$, (ZA) (99.9%, Merck Co.) was dissolved in 50 ml of methanol, CH_4O, (99 %, SDFCL company, India) under vigorous stirring at 60 ^oC for 30 min followed by sonication for 20 min. A clear and transparent homogenous solution was obtained. Some drops of 5M NaOH aqueous solution was added drop-wise into the acetate solution under vigorous stirring until pH became 14. The colorless homogenous solution changed to milky white slurry colloidal. The colloidal was heated under vigorous stirring for 1 hr. at 60 ^oC. Then, the colloidal was stirred slowly at room temperature for 12 hrs. The colloidal was, subsequently, transferred to 100 ml Teflon lined stainless steel autoclave reactor for 3 hrs. at 160 ^oC. After that, a white precipitate was carefully collected and then, centrifuged at 3500 rpm by washing 5 times for 1.5 hrs. using absolute ethanol to remove the sodium acetate and non-reacted materials [20]. Then, the product was dried at 65^oC overnight. Finally, the powder was crashed gently using mortar and pestle to produce fine powder.

- **Sol-Gel Method**

Sol–gel (SG) process generally undergoes in four stages: salvation, hydrolysis, polymerization and transformation into ZnO solid powder [21]. 2.7 g of ZA was dissolved into 35 ml of absolute methanol (Me), under vigorous stirring for 30 min at 60 ^oC followed by sonication for 15 min until clear and transparence solution was found. In the same way, 3.15 g of oxalic acid (OA) ($H_2HTO_4.2H_2O$, 99.5%, Merck Co.) was dissolved into 10 ml of tribal distilled water at 60 ^oC and it was kept under constant stirring for 15 min to dissolve completely. OA solution that acted as precipitation agent was added as a dropwise to the ZA solution under vigorous stirring. White gel was formed and the stirring continued at 60 ^oC for 1 hr. The colloidal left at room temperature for 12 hrs. under slow stirring. The product gel was washed 5 times using absolute ethanol to remove the unreacted materials using centrifugation at 3500 rpm [20]. Then, the product was heated at 90 ^oC for 12 hrs. The gel was calcinated at about 400 ^oC for 1 hr. Finally, the product was crashed gently using mortar and pestle to produce fine powder before use. Fig. 1 illustrates the procedures of synthesis the ZnO NPs by HT and SG methods.

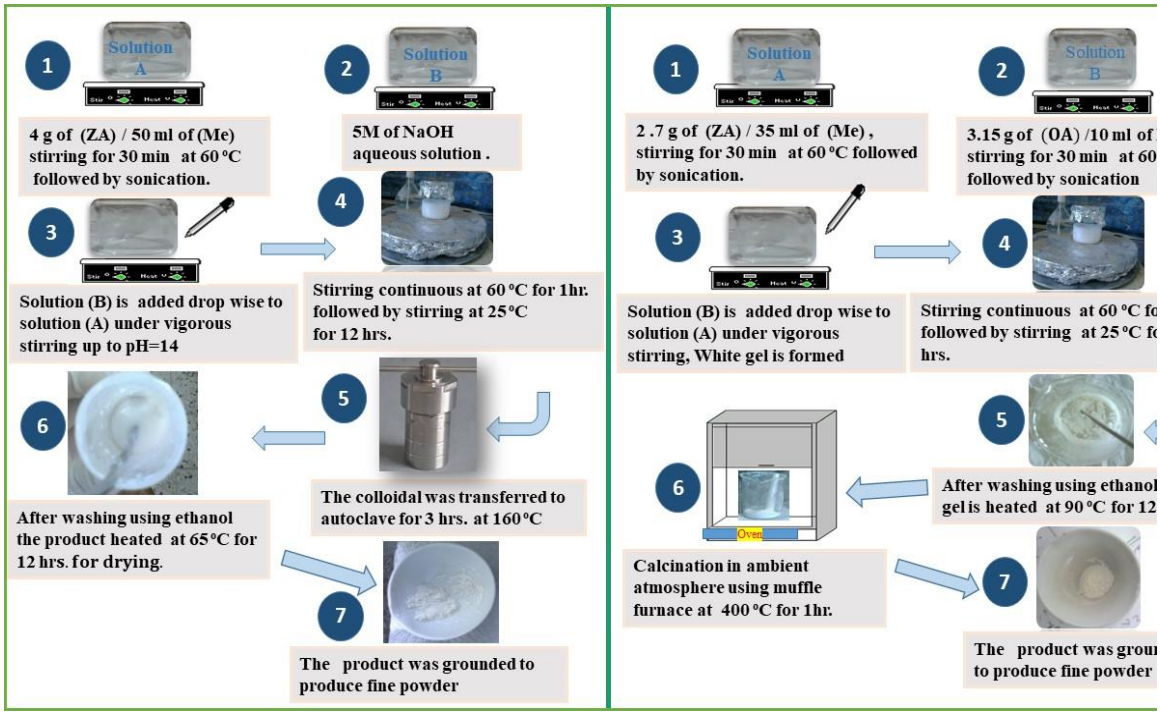

1. Hydrothermal method **2. Sol-gel method**

Figure 1: Flowchart for the synthesis process of ZnO NPs using two different chemical methods.

2.2 Characterization and Photoelectric Measurements

The crystal geometrical identification and crystal size analysis were examined by X ray diffraction (XRD) (40 kV, step size 0.03, scan rate 0.5 min^{-1}, $15^{\circ} \leq 2\theta \leq 80^{\circ}$) using Philips Expert, XRD equipped with Cu-K_{α} radiation (λ=1.5418 A°). High-resolution transmission electron microscopy analysis (HRTEM) was performed with (JEM-2100), 200 kV. Field Emission Scanning Electron Microscope (FESEM) (Type Quanta FEG 250) Philips attached with electron dispersive x- ray detector (EDX) was conducted to find out the accurate composition of the invested samples. The UV–VIS absorption spectra of synthesized powder were tested in ethanolic solutions and performed using double beam shimadzu UV-1601 PC. Photoluminescence (PL) emission spectra was measured in ethanolic media at room temperature with spectrofluorimeter model SPF-200 (Biotech Engineering Management Co., UK) in the range from 350 nm to 800 nm with excitation wavelength 320 nm. The photovoltaic DSSCs devices were characterized using an AM 1.5(100 $mWcm^{-2}$) sunlight simulator. The solar cell sample was conducted with (Elvis national instruments in combination with the LabVIEW program). The J-V curves of the fabricated DSSCs were obtained by applying an external reverse bias voltage in the range -1 to 1 to the solar cell. To measure the adsorbed dye on the ZnO NPs photoanode films, the dye was desorbed by immersing dye-sensitized films in a 0.1 M NaOH solution in H_2O and ethanol (50:50, v/v). An UV-VIS spectrophotometer was employed to measure the dye concentration of the desorbed dye solution. The amount of the adsorbed dye on ZnO NPs layer was estimated from the absorption spectra of the absorb dye from the colored ZnO NPs layer.

3 Results and Discussion

3.1 Characterization Studies

3.1.1 Energy Dispersive X-ray Analysis (EDX)

The composition of the prepared ZnO NPs samples was investigated using EDX analysis. Typical EDX spectra are shown in Fig.2. The spectra reveal that in the case of SG technique only two elements, Zn

and O were existed with higher concentration. However, in the case of HT technique a very small concentration of carbon appeared, in addition to, Zn and O elements. The obtained results correspond to the finding done by S. Brita *et al.* [22]

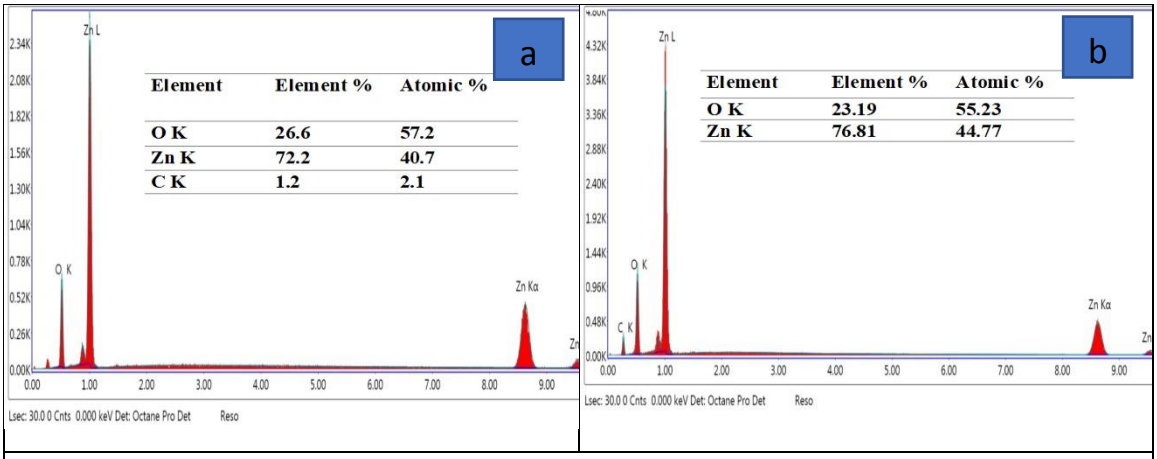

Figure 2: EDX spectra of the synthesized ZnO NPs by (a) Hydrothermal and (b) Sol gel method.

3.1.2 X-ray diffraction studies

The XRD pattern for the prepared HT and SG samples are shown in the Fig. 3. The XRD pattern of the prepared samples match with the standard (ICSD card No. 067454). ZnO NPs crystal have been grown with hexagonal phase, wurtzite structure with lattice parameters, as given in Table 1. No other phases have been observed, which further confirmed the formation of ZnO NPs with single phase. These diffraction peaks are significantly broadened due to the small size of the NPs [23]. The sharpness of the diffraction peaks indicates to the good crystallinity. The particle size (D) was estimated from the broadening of the highest intensity peak (101) plane by using the Debye-Scherrer's formula [24].

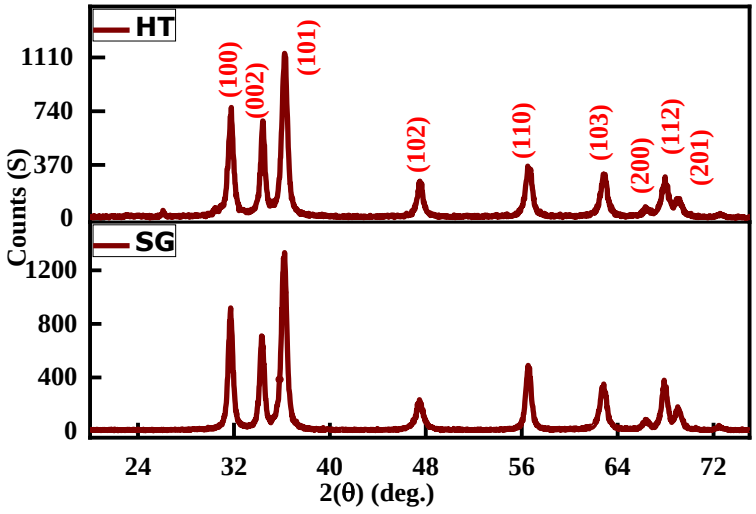

Figure 3: X-ray diffraction pattern of HT and SG samples.

Table 1: Geometric parameters for HT and SG samples.

Sample	a(nm)	c(nm)	c/a	V_{UC} x10^{-3} $(nm)^{-3}$	D (nm)
HT	3.249	5.206	1.602	47.599	27.93
SG	3.239	5.203	1.606	47.277	24.70

3.1.3 HRTEM analysis of ZnO NPs.

The morphology of the ZnO NPs was examined by high-resolution transmission electron microscopy (HRTEM). Fig. 4 and Fig. 5 depict the HRTEM images for HT and SG ZnO NPs samples, receptively, (a) micrograph image, (b) Diffraction patterns, (c) selected electron diffraction area (SAED) and (d) histograms. As shown in these figures, the synthesized ZnO NPs are good in the crystalline, and semispherical in shape with particle size 25.3 and 22.3 nm for the samples HT and SG, respectively, which closes to the estimated particle size from the XRD pattern. The spacing between the adjacent lattice planes (d) of ZnO NPs was calculated from the bright field SAED patterns about 0.246 nm and 0.215 nm for the samples HT and SG, respectively. These results match with the calculated results from XRD and corresponded to the (101) of ZnO NPs, also, agree with Hasan et al [25]

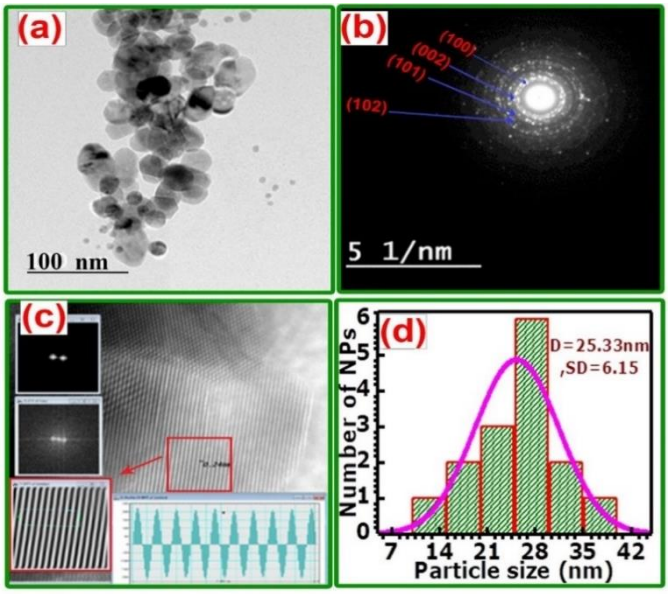

Figure 4: HRTEM micrograph of (HT) ZnO NPs sample (a) micrograph image, (b) Diffraction patterns (c) selected electron diffraction area and (d) histograms.

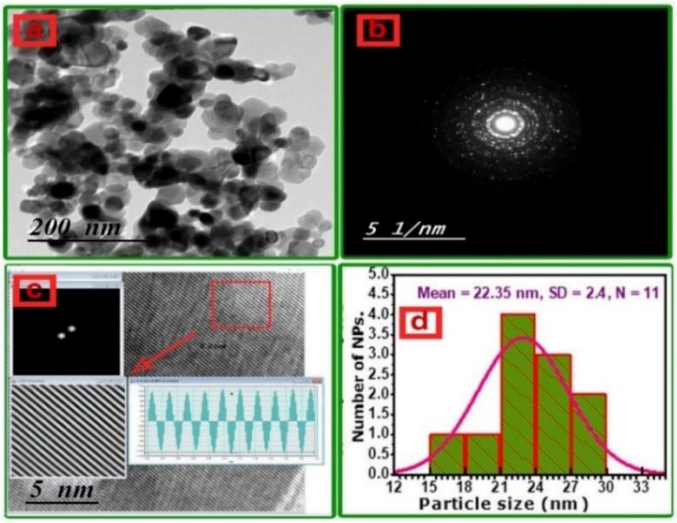

Figure 5: HRTEM micrograph of (SG) ZnO NPs sample (a) micrograph image, (b) Diffraction patterns (c) selected electron diffraction area and (d) histograms.

3.2 Optical studies of ZnO NPs

3.2.1 UV-VIS absorption studies

The optical properties of the synthesized ZnO NPs were studied by UV-VIS absorption spectroscopy. Fig. 6(a) depicts that, ZnO NPs have a high absorbance in the UV region and then they decrease exponentially with the increasing of wavelength. In addition, this figure demonstrates that ZnO NPs have high transparency in the visible region. Furthermore, the corresponding absorption edge was observed at, 360.8 nm and 375.8 nm for the samples HT and SG, respectively, which are less than the standard UV absorption peak of bulk ZnO at 388 nm [26]. With respect to the bulk ZnO, it is clear that, the absorption peak shifted to low wavelength. This shift was attributed to quantum confinement effect [27, 28]. Optical energy band gap can be estimated from the intercept of linear portion of the curve on x-axis that is represented by energy (hν). It is seen from Fig.6(b) that, the estimated optical energy band gaps (Eg) 3.13 eV and 3.16 eV for the samples HT and SG, respectively, which are agreed well with refs. [16, 29].

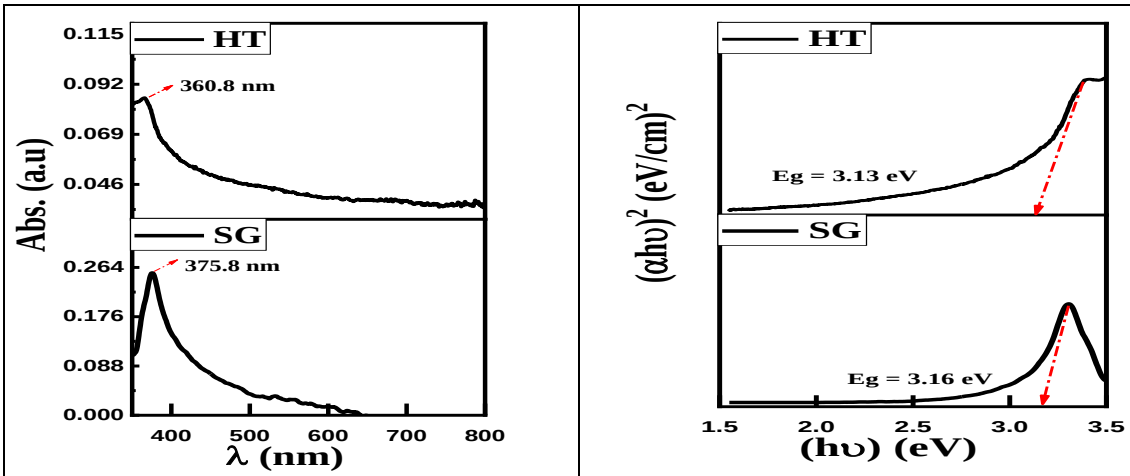

Figure 6: Variation of absorption spectra and optical energy gap of the two synthesised samples.

3.2.1 Photoluminescence spectroscopy of pure ZnO NPs

Fig. 7 shows the PL emission spectrum (PLES) of prepared HT and SG samples, which were excited at 320 nm. The main features of the PLES of ZnO NPs can be decomposed into Near-Ultraviolet (NUV) region and visible region i.e. violet-blue (VB), blue-green (BG) and orange-red (OR). The NBE of ZnO NPs typically exhibits a linear emission in the range (originating from exciton mechanism) where in the visible region, it is connected to defects in ZnO NPs or interior energy traps (IETs) [30]. The PLES of NUV region, which are positioned near band edge (NBE) emission, are due to the radiative recombination of free excitons through an exciton–exciton collision process [31]. The large exciton binding energy of ZnO allows an intense NBE excitonic emission at room temperature and higher temperatures [32]. It can be seen from Fig. 7 that intensity of the VB emission for HT is higher than the VB emission for SG. Different types of IETs are presumed to explain the observed emission bands in the visible range. The VB emission peaks are assigned to the transition of electron from the bottom (donor) of conduction band to the energy level of Zn vacancy (V_{Zn}), which infers that the ZnO NPs are n-type semiconductors [33]. The BG emission is caused by the transition of electrons from conduction band edge to the IETs complex (V_{ZnO}) [34]. Generally, the OR is attributed to deep IETs interstitial and vacancies of oxygen (O_i and V_o), respectively, in ZnO NPs [31, 35]. The inset in Fig. 7 reveals that a blue shift occurred in the PLES spectra of the samples HT, which is in good agreement with the previously obtained UV-VIS results.

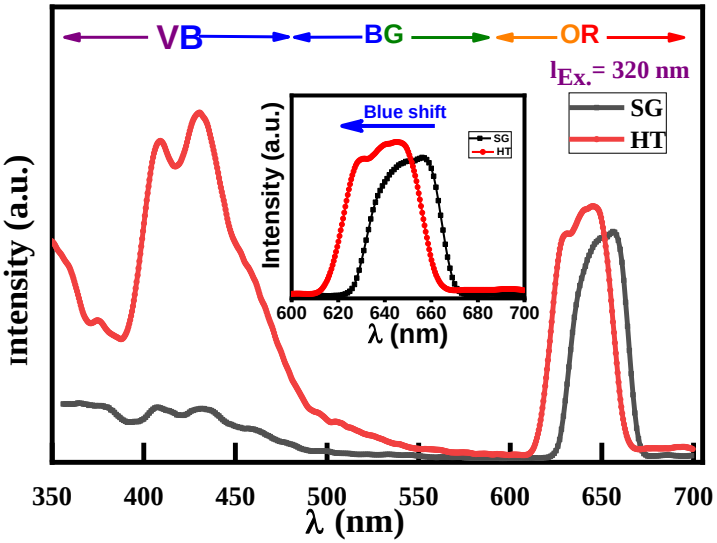

Figure 7: PL spectra of HT and SG samples

3.3 Photovoltaic parameters

Fig.8 and Fig.9 illustrates the variation of the current density - voltage (J-V) characteristic curves for the DSSCs. As clearly presented in all J-V characteristic curves, all curves are found to have the shape of diode's characteristic curve. All the photovoltaic parameters of the fabricated DSSCs were calculated from the J-V curves and then were listed in the Table 2. As displayed in Table 2, open circuit voltage (V_{oc}) values varied from 0.37-0.51 V. The highest V_{oc} was obtained for the DSSC of the SG sample that was sensitized with EY and the lowest one was obtained for the DSSC of the HT sample that was sensitized with EB. These values depend on the difference between Fermi energy (E_f) level and energy of redox (E_{redox}) level. Short circuit current density (J_{sc}) values vary from 0.51 to 4.97 mA/cm^{-2}. Remarkable high J_{sc} of 4.97 and 4.25 mAcm^{-2} were obtained for the DSSCs of the HT and the SG samples sensitized with EY, respectively. The higher value of J_{sc} of HT sample dyed by EY may be attributed to the surface structure of the electrode, the amount of dyes adsorbed on the surface, or the electron injection ability[36]. The Fill factor (FF) of the fabricated DSSC ranged between 49.76% and 53.8%. The FF was obtained from the DSSCs sensitized with the EB has the lowest value, this may be attributed to low shunt resistance or large series resistance [37]. The lowest efficiency (η) value and lowest performance were found for the HT DSSC sensitized with EB which has the following results, V_{oc} = 0.37 V, J_{sc} = 1.60 mAcm^{-2}, P_m = 0.29 mWcm^{-2}, FF = 49.76 %, and η =

0.29 %. This performs may be attributed to weak bonding between the dye molecule and ZnO particles and less of dye adsorption. But in case of EY and RB photosensitizer, HT exhibit improved performance. The best performance was obtained from the DSSC sensitized by the EY, which has the following result: V_{oc} = 0.51 V, J_{sc} = 4.25 mAcm^{-2}, P_m = 1.08mWcm^{-2}, FF = 50.08 %, and the efficiency of the cell reached 1.08 %. These results are comparable than those obtained for the DSSCs sensitized by other low cost sensitizer dyes [36, 38]. The obtained results showed an enhancement of both the J_{sc} and the V_{oc} of the EY rather than that of the EB and RB, which may be attributed to broader range of absorption with respect to the others, and it, has higher intensity as depicted in Fig. 10. In addition, EY has the higher dye uploading on the surface of the ZnO NPs. Absorption spectra of EB, EY and RB dyes were desorbed from ZnO NPs semiconductor layer as depicted in Fig. 9. This leads to harvest high amount of photo energy of the sun light.

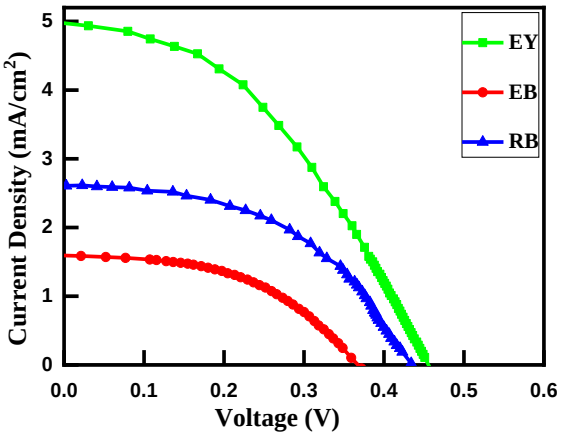

Figure 8: J-V characteristic curves of the DSSCs HT of pure ZnO NPs, using different dyes.

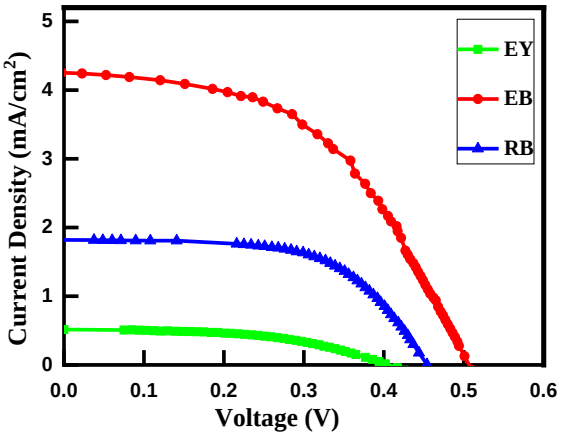

Figure 9: J-V characteristic curves of the DSSCs SG of pure ZnO NPs, using different dyes.

Table 2: Photovoltaic parameters of the DSSCs fabricated using HT and SG samples

Sample	Dye	J_{sc}(mA/cm^2)	V_{oc}(V)	J_m (mA/cm^2)	V_m (V)	P_m (mW/cm^2)	FF%	η%
HT	EB	1.60	0.37	1.15	0.25	0.29	49.76	0.29
SG		0.52	0.41	0.39	0.28	0.11	50.62	0.12
HT	EY	4.97	0.46	3.51	0.27	0.94	41.46	0.94
SG		4.25	0.51	3.19	0.34	1.08	50.08	1.08
HT	RB	2.62	0.44	1.97	0.29	0.56	48.65	0.56
SG		1.85	0.45	1.94	0.37	0.72	53.80	0.72

3.3.1 Dye uploading

Fig. 10 depicts the UV-VIS absorption spectra of EB, EY and RB. This Figure, shows that the maximum absorption peak of EY, EB and RB at 526 nm, 534 nm, and 543.5 nm, respectively. EY exhibits a powerful absorption peak in the visible region and its spectrum covers broader window compare to the others. The difference in the absorption characteristics is due to the different of colors of the dyes. The observed absorption peaks in the spectral range between 449 nm and 582 nm represent a part of energy losses in the transition in the UV region. In the DSSCs application, it is much of interests to concentrate in the visible solar spectrum. In addition, to that the molar extinction coefficient of EY equals 112,000 (cmM)$^{-1}$ [39] which is greater than that of RB (106,000 (cmM)$^{-1}$) [40] and much higher than that of EB (50620 (cmM)$^{-1}$) [41], corresponding to $\pi \rightarrow \pi^*$ transitions of conjugated molecules. This may explain the higher performance of DSSCs using EY above that using of other dyes. The spectra of EB, EY and RB dyes were desorbed from

ZnO NPs semiconductor layer was depicted in Fig.11. The absorption spectrum of the adsorbed dyes on to ZnO NPs film is obviously wider and very little shifted to the lower wavelength compared with the absorption spectra of the dye solution, which indicates that, there is interaction between the dye molecules and the cationic ZnO NPs surface. This interaction means that the anchoring of EY on the ZnO NPs surface are ideal compare to the others. It can be seen that the absorption peaks at about 526 nm, 517.47 nm and 550.9 nm for EY, EB and RB, respectively. The area under curves for EB, EY and RB in the visible region (400-800) are about 66.40, 31.70 and 38.39 for EY, EB and RB, respectively. This reflects the variation of the performance of the DSSCs. The area under the curve of EY is about twice the value of RB, which exhibits the best efficiency; on the other hand, EB has the least area under curve, which has the lowest conversion efficiency.

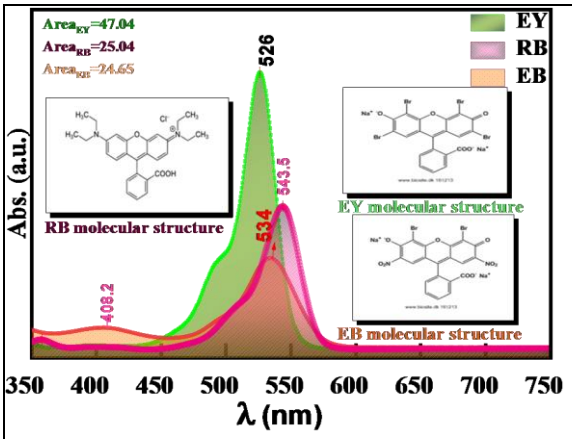

Figure 10: The absorption spectrum of the used dyes dissolved in pure ethanol

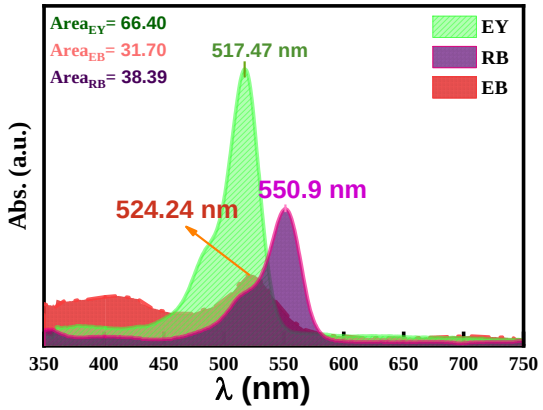

Figure 11: Absorption spectra of EB, EY and RB dyes were desorbed from ZnO NPs semiconductor layer.

4 Conclusion

In this study, highly purity wurtzite hexagonal phase of ZnO NPs were synthesized by hydrothermal and sol-gel techniques. The calculated particle size, from XRD was in the range 25-28 nm. The morphology of ZnO NPs was semispherical shape. UV-VIS results reveled that ZnO NPs has strong absorption in UV region. In addition, the band gap for the prepared samples were 3.13 eV and 3.16 eV for HT and SG sample respectively. Three chemical dyes were used as photosensitizers for DSSCs. The absorption spectra revels that EY has the highest absorption. The J-V characteristic curves of all fabricated cells were measured and analyzed. The parameters related to the cell performance were presented. Moreover. The best performance was obtained for the DSSC sensitized with EY where, the photovoltaic parameters of J_{sc} = 4.25 (mA/cm^2), V_{oc} = 0.51 V and η=1.08 %.

Acknowledgments

This research activity carried out between Gaza-Palestine and Cairo-Egypt, which was financially supported by Qatar Charity IBHATH Project grant funded by the Gulf Cooperation Council for the Reconstruction of Gaza through the Islamic Development Bank.

CONFLICT OF INTERESTS.

- There are no conflicts of interest.

References

[1] S. Preethi, A. A. a. M. A, A Comparative Analysis of the Properties of Zinc Oxide (ZnO) Nanoparticles Synthesized by Hydrothermal and Sol-Gel Methods, *Indian Journal of Science and Technology*, 2016, 9, (40), pp. 1-6

[2] Zhang, L. and A. Konno, Development of Flexible Dye-sensitized Solar Cell Based on Pre-dyed Zinc Oxide Nanoparticle, *International Journal of Electrochemical Science*, 2018, 13, (1), pp. 344-352.

[3] A.B Djurisic A. M. C. Ng and X. y. Chen., ZnO Nanostructures for Optoelectronics: *material properties and device applications, Progress in Quantum Electron.*, 2006. 34(191), pp. 191-259.

[4] Nunes, V. F.; Souza, A. P. S.; Lima, F.; Oliveira, G.; Freire, F. N.; Almeida, A. F., Effects of Potential Deposition on the Parameters of ZnO Dye-Sensitized Solar Cells, *Materials Research*, 2018, 21, (4), pp.1-8.

[5] Düring, J.; Kunzmann, A.; Killian, M. S.; Costa, R. D.; Guldi, D. M.; Gröhn, F., Porphyrins as Multifunctional Interconnects in Networks of ZnO Nanoparticles and Their Application in Dye-Sensitized Solar Cells, *ChemPhotoChem*, 2018, 2, (3), pp. 213-222.

[6] S.Y.H. Abdalkarim, H.-Y. Yu, C. Wang, L. Yang, Y. Guan, L. Huang, J. Yao, Sheet-like cellulose nanocrystal-ZnO nanohybrids as multifunctional reinforcing agents in biopolyester composite nanofibers with ultrahigh UV-Shielding and antibacterial performances, *ACS Applied Bio Materials*, 2008, 4, (11), pp,11-37.

[7] Nagaraju, G.; Shivaraju, G.; Banuprakash, G.; Rangappa, D., Photocatalytic activity of ZnO nanoparticles: synthesis via solution combustion method, *Materials Today: Proceedings*, 2017, 4, (11), pp. 11700-11705.

[8] Periyayya Uthirakumar , H.G.K., Chang-Hee Hong, Zinc Oxide Nanostructures Derived From A simple Solution Method for Solar Cells and LEDs, *Chemical Engineering Journal*, 2009, 155, (1). pp. 910-915.

[9] Hsu, M.-H.; Chang, S.-P.; Chang, S.-J.; Li, C.-W.; Li, J.-Y.; Lin, C.-C., Fabrication of Zinc Oxide-Based Thin-Film Transistors By Radio Frequency Sputtering for Ultraviolet Sensing Applications, *Journal of nanoscience and nanotechnology*, 2018, 18, (5), pp. 3518-3522.

[10] Acosta, D.; López-Suárez, A.; Magaña, C.; Hernández, F., Structural, Electrical and Optical Properties of ZnO Thin Films Produced by Chemical Spray Using Ethanol in Different Amounts of The Sprayed Solution, *Thin Solid Films*, 2018, 653, (1), pp. 309-316.

[11] Menzel, A.; Komin, K.; Yang, Y.; Güder, F.; Trouillet, V.; Werner, P.; Zacharias, M., Ultra-long Zinc Oxide Nanowires and Boron Doping Based on Ionic Liquid Assisted Thermal Chemical Vapor Deposition Growth, *Nanoscale*, 2015. 7(1), pp. 92-97.

[12] Krämer, A.; Engel, S.; Sangiorgi, N.; Sanson, A.; Bartolomé, J. F.; Gräf, S.; Müller, F. A., ZnO Thin Films on Single Carbon Fibres Fabricated by Pulsed Laser Deposition (PLD), *Applied Surface Science*, 2017, 399, (1), pp. 282-287.

[13] Dobrozhan, O.; Kurbatov, D.; Opanasyuk, A.; Cheong, H.; Cabot, A., Influence of Substrate Temperature on The Structural and Optical Properties of Crystalline ZnO Films Obtained by Pulsed Spray Pyrolysis, *Surface and Interface Analysis*, 2015, 47(5), pp. 601-606.

[14] Barhoum, A.; Van Assche, G.; Rahier, H.; Fleisch, M.; Bals, S.; Delplancked, M.-P.; Leroux, F.; Bahnemann, D., Sol-Gel Hot Injection Synthesis of ZnO Nanoparticles into a Porous Silica Matrix and Reaction Mechanism, *Materials & design*, 2017, 119, (1), pp. 270-276.

[15] Silambarasan, M., S. Saravanan, and T. Soga, Effect of Fe-Doping on The Structural, Morphological and Optical Properties of ZnO Nanoparticles Synthesized by Solution Combustion Process, *Physica E: Low-dimensional Systems and Nanostructures*, 2015, 71, (1), pp. 109-116.

[16] Shaat, S.; Zayed, H.; Musleh, H.; Shurrab, N.; Issa, A.; Asad, J.; Al Dahoudi, N., Inexpensive Organic Dyes-Sensitized Zinc Oxide Nanoparticles Photoanode for Solar Cells Devices, *Journal of Photonics for Energy*, 2017, 7, (2), pp. 1-15.

[17] Naji M. AlDahoudi, S. A. S., Nabil K. Shurrab, Ahmed A. Issa, Hussam S. Musleh, Jehad A. Asaad, Hamdia A. Zayed., Influence of Metal Ion Doping of Zinc Oxide Photoanode on The Efficiency of Dye Sensitized Solar Cell. *IUG Journal of Natural Studies*, 2017, 1, (1), p. 155-159.

[18] Talaat M. Hammad, J.K.S., R. G. Harrison, Structure, Optical Properties and Synthesis of Co-Doped ZnO, *superstructures,Appl Nanosci*, 2012. 1(1), pp. 1-7.

[19] Do, T. T.; Hoang, T. H.; Do, T. A. T.; Pham, Q. N.; Giang, H .T.; Bui, H. T.; Tran, T.; Ho, T. G, Correlation Between Optical Characteristics and NO_2 Gas Sensing Performance of ZnO Nanorods Under UV Assistance. *Vietnam Journal of Science, Technology and Engineering*, 2018, 60, (1), pp. 68-72.

[20] Hammad, T.M., J.K. Salem, and R.G. Harrison, The Influence of Annealing Temperature on The Structure, Morphologies and Optical Properties of ZnO Nanoparticles, *Superlattices and Microstructures*, 2010, 47, (2), pp. 335-340.

[21] Alias, S., A. Ismail, and A. Mohamad, Effect of pH on ZnO Nanoparticle Properties Synthesized by Sol–Gel Centrifugation, *Journal of Alloys and Compounds*, 2010, 499 ،(2), pp. 231-237.

[22] Brintha, S. and M. Ajitha, Synthesis and Characterization of ZnO Nanoparticles Via Aqueous Solution, Sol-gel and Hydrothermal Methods, *IOSR Journal of Applied Chemistry*, 2015, 8, (11): pp. 66-72.

[23] Talaat M. Hammad, J.K.S., Roger G. Harrison The influence of annealing temperature on the structure,morphologies and optical properties of ZnO nanoparticles, *Superlattices and Microstructures*, 2010, 1, (47), pp. 335-340.

[24] Zak, A.K. and W.A. Majid, Characterization and X-ray peak broadening analysis in PZT nanoparticles prepared by modified sol–gel method. *Ceramics International*, 2010, 36, (6), pp. 1905-1910.

[25] Hasan, K.; Alvi, N.; Lu, J.; Nur, O.; Willander, M., Single nanowire-based UV photodetectors for fast switching. *Nanoscale research letters*, 2011, 6, (348), pp. 1-6

[26]Tapas Kumar Kundu, N.K., Puspendu Barik , Satyajit Saha, Optical Properties of Zno Nanoparticles Prepared by Chemical Method Using Poly (VinylAlcohol) (PVA) as Capping Ag. *International Journal of Soft Computing and Engineering*, 2011, 1, (1), pp. 19-24.

[27] Fang-I Lai , J.-F.Y.a.S.-Y.K., Efficiency Enhancement of Dye-Sensitized Solar Cells' Performance with ZnO Nanorods Grown by Low-Temperature Hydrothermal Reaction. *Materials*, 2015, 8,(1): pp. 8860–8867.

[28]Harish Kumar, R.R., Structural and Optical Characterization of ZnO Nanoparticles Synthesized by Microemulsion Route, *International Letters of Chemistry, Physics and Astronomy*, 2013, 14, (1), pp. 26-36.

[29] S. S. Kanmani, K.R., and S. Umapathy, Eosin Yellowish Dye-Sensitized ZnO Nanostructure-Based Solar Cells Employing Solid PEO Redox Couple Electrolyte, *International Journal of Photoenergy*, 2012, 1, (1), pp. 1-8.

[30] Ghosh, M. and A. Raychaudhuri, Shape transition in ZnO nanostructures and its effect on blue-green photoluminescence, *Nanotechnology*, 2008, 19, (44), pp. 1-16

[31] Kumar, V.; Swart, H. C.; Ntwaeaborwa, O. M.; Kroon, R. E.; Terblans, J. J.; Shaat, S. K. K.; Yousif, A.; Duvenhage, M. M., Origin of the red emission in zinc oxide nanophosphors, *Materials Letters*, 2013, 101, (1), pp. 57-60.

[32] Robina Ashraf, S.R., Muhammad Khaleeq-ur-Rehman and Shahzad Naseem, Synthesis and Characterization of ZnO Nanoparticles. *The 2013 world Congress on Advances in Nano, Biomechanics, Robotics and Energy Research Seoul, Korea*, 2013, 25, (28), pp.1-8

[33] Lin, J.-H.; Patil, R. A.; Devan, R. S.; Liu, Z.-A.; Wang, Y.-P.; Ho, C.-H.; Liou, Y.; Ma, Y.-R., Photoluminescence mechanisms of metallic Zn nanospheres, semiconducting ZnO nanoballoons, and metal-semiconductor Zn/ZnO nanospheres, *Scientific reports*, 2014. 4.

[34]Shakti, N.; Prakash, A.; Mandal, T.; Katiyar, M., Processing temperature dependent morphological and optical properties of ZnO nanorods. *Materials Science in Semiconductor Processing*, 2014, 20,(1), pp. 55-60.

[35] Lim, K.; Abdul Hamid, M. A.; Shamsudin, R.; Al-Hardan, N.; Mansor, I.; Chiu, W., Temperature-driven structural and morphological evolution of zinc oxide nano-coalesced microstructures and its defect-related photoluminescence properties, *Materials*, 2016, 9, (4), pp. 1- 15.

[36] Pipat Ruankham, C.S., Nikorn Mangkorntong, Pongsri Mangkorntong, Supab Choopun, Photoelectrochemical Characteristic of ZnO Dye-sensitized Solar Cell with Platinum Nanoparticle as a Counterelectrode. *Chiang Mai University. Journal of Natural Sciences, Special Issue on Nanotechnology*, 2008, 7, (1), pp.

[37] Halme, J., Dye-sensitized nanostructured and organic photovoltaic cells: technical review and preliminary tests. Master of Science in Technology, Helsinki University of Technology, Helsinki, Finland, 2002.

[38] H. A. Zayed, H. Musleh S. Shaat, A. Issa, N. Shurrab, J. Asaad, N. AlDahoudi, Synthesis of Zinc Oxide nanoparticles at different aging time for low cost Dye Sensitized Solar Cells, *Journal of Scientific Research for Science*, 2017,(34) ,pp 23-36

[39] Dixon, J.M., M. Taniguchi, and J.S. Lindsey, PhotochemCAD 2: a refined program with accompanying spectral databases for photochemical calculations, *Photochemistry and photobiology*, 2005, 81, (1), pp, 212-213.

[40] https://omlc.org/spectra/PhotochemCAD/html/009.html, Eastman Laboratory Chemicals Catalog No. 55 (1993-94), F.S.h.o.o.s.P.d.-a.

[41]Math ،N.; Naik, L.; Suresh, H.; Inamdar, S., Dual fluorescence and laser emissions from fluorescein-Na and eosin-B. *Journal of luminescence*, 2006, 121, (2), pp. 475-487.

تخليق ودراسة خصائص جسيمات نانوية من أكسيد الزنك باستخدام طريقة الهيدروثيرمال وطريقة الصول جل واستخدامها في صناعة خلايا شمسية صبغية

حسام مصلح [1،2] ناجي الداهودي[2] حمدية عبد الحميد زايد[1] سامي شعث[3]

حسن طموس[4] نبيل شراب[4] أحمد عيسي[5] جهاد أسعد[2] أمل الكحلوت[2]

(1) كلية البنات للاداب والعلوم والتربية – جامعة عين شمس – القاهرة – مصر

(2) قسم الفيزياء– جامعة الازهر–غزة– فلسطين

(3) قسم الفيزياء –الجامعة الاسلامية–غزة – فلسطين

(4) قسم الكيمياء –جامعة الازهر – غزة – فلسطين

(5) كلية الهندسة–جامعة الازهر –غزة – فلسطين

الخلاصة

في هذا البحث تم تخليق جسيمات نانوية نقية من أكسيد الزنك باستخدام طريقتي الهيدروثيرمال وطريقة الصول جل. من فحوصات حيود الاشعة السينية تبين أن متوسط حجم الحبيبة تتراوح بين من 25 الي 28 نانومتر وتاخذ شكلا كرويا. فحوصات طيف الامتصاص بينت أن العينات جميعها لها اعلي امتصاص في منطقة الاشعة الفوق بنفسجية. وتم حساب فجوة الطاقة للعينات فوجد انها تساوي 3.13 eV و3.16 eV للعينة التي حضرت بطريقة الهيدروثيرمال والصول جل على الترتيب. تم تحضير عينات لخلايا شمسية صبغية وتم استخدام 3 انواع من الاصباغ الكيمياءية كمتحسسات ضوئية. فحوصات الاشعة الفوق بنفسجية بينت ان صبغة الايوزين الاصفر Eosin Yتعطي اعلي امتصاص مقارنة بالاصباغ المستخدمة الاخري. تم رسم منحني الخواص لجميع العينات للخلايا الشمسية المحضرة وتم حساب جميع البارامترات اللازمة لتقييم اداء الخلية. العينة المصبوغة بصبغةEosin Y اعطت اعلي كفاءة(J_{sc} = 4.25 (mA/cm^2) ، V_{oc} = 0.51 V and η=1.08 %

كلمات الداله: أكسيد زنك نانوي، طريقة صول جل، طريقة هيدروثيرمال، وميض ضوئي، خلايا شمسية صبغية.